ACTA GEODYNAMICA ET GEOMATERIALIA

ORIGINAL PAPER

MONTE CARLO MSSA TO MODELING GNSS POSITION TIME SERIES AND ITS IMPLICATION FOR CRUSTAL DEFORMATION MONITORING

Yunfei XIANG [1] *, Jianping YUE [2], Guoliang LIU [1] and Yuxiang LONG [1]

[1] *Department of Geomatics Engineering, Nanjing Forestry University, Nanjing 210037, China*
[2] *School of Earth Sciences and Engineering, Hohai University, Nanjing 211100, China*

Corresponding author's e-mail: yfxiang@njfu.edu.cn

ABSTRACT

In this paper, a scheme of signal extraction and modeling for GNSS position time series based on Monte Carlo Multi-channel Singular Spectrum Analysis (MC-MSSA) is introduced, which can effectively consider the spatial correlation of different directions by processing the different components of position time series at the same time. Meanwhile, the Monte Carlo significance test is utilized to distinguish the signal from the colored noise. By comparing with Singular Spectrum Analysis (SSA), it can be confirmed that MSSA has better signal extraction and modeling performance by taking into account the correlation of different channels. Then, taking the LHAZ station as an example, MC-MSSA is utilized to simultaneously model the three components of GNSS position time series, and the trend and periodic signals are respectively identified by Kendall nonparametric test and W-correlation correlation analysis. The result denotes that MC-MSSA can effectively model the tectonic and non-tectonic signals of GNSS position time series, and the modeled signals can more intuitively reflect the dynamic movement of the station. Finally, based on the MC-MSSA-modeled tectonic signal, we characterize the crustal deformations around the eastern Tibetan Plateau, mainly including the crustal movement and strain rate change. The results suggest that the pushing movement of the Tibetan Plateau from the Indian plate is blocked by the South China block, and the crustal movement rate is obviously decreased and appears a right-handed movement trend. Meanwhile, the junction of the Tibetan Plateau and South China block has accumulated a certain amount of stress, and the tectonic activity at the junction is relatively strong and still belongs to the dangerous zone of seismic activity.

1. INTRODUCTION

GNSS position time series records the dynamic movement of the station along time, which contains a wealth of tectonic and non-tectonic information, providing important data for related research in the geodesy field (Blewitt et al., 2001; Bock et al., 2016; Wu et al., 2017; Pan et al., 2017; Pan et al., 2019). In the field of seismology, the entire earthquake cycle can be divided into three phases: co-seismic, inter-seismic, and post-seismic (Elliott et al., 2016b; Feigl and Thatcher, 2006). The elastic rebound theory denotes that the plate moves relative to each other and gradually accumulates tectonic stress during the inter-seismic phase (Savage and Lisowski, 1993). When the accumulated tectonic stress is greater than the limit of the lithosphere, the lithosphere will rupture sharply, causing the occurrence of earthquake. During the post-seismic phase, the energy is further released, and the crust jumps back to its pre-seismic state to start a new round of stress accumulation and release. For the inter-seismic phase, the GNSS position time series mainly reflects the tectonic movements and the non-tectonic deformations caused by geophysical factors (i.e., atmospheric pressure, non-tidal oceanic changes,

and hydrological loading). The research of GNSS position time series modeling method is of great significance not only for characterizing the regional crustal movement in the inter-seismic phase, but also for the establishment and maintenance of the dynamic reference frame (Dietrichet al., 2001; Altamimi et al., 2011). Thus, it is necessary to carry out research on the signal extraction and modeling method of GNSS position time series during the inter-seismic phase.

In general, GNSS position time series contains different signal components. How to accurately and effectively extract different signals with considering of the influence of colored noise is an important issue (Wang et al., 2016; Ming et al., 2016; He et al., 2017). Currently, the GNSS position time series modeling methods contain wavelet analysis, Least Square Fitting (LSF), SSA (Chen et al., 2013; Li et al., 2017), Kalman Filtering (KF) (Davis et al., 2012; Liu et al., 2017), Empirical Mode Decomposition (EMD) (Montillet et al., 2013), Ensemble Empirical Mode Decomposition (EEMD) (Lian et al., 2012), and Complementary Ensemble Empirical Mode Decomposition (CEEMD) (Wang et al., 2015, He et al., 2020), etc. Among them, SSA is an effective signal

extraction and modeling method, which can extract signals from noisy position time series without any prior information. Chen et al. (2013) utilized SSA to model the seasonal signal of GNSS position time series, and compared it with KF and LSF to prove that SSA is an effective method to extract time-varying seasonal oscillation signals. Gruszczynska et al. (2015) demonstrated that SSA can effectively extract and model the signal in the GNSS position time series without prior information by comparing SSA with LSF. Li et al. (2017) also verified that SSA can capture the peak of seasonal signals in GNSS observations, while cannot be accurately detect by LSF. However, SSA only analyzes the dynamic variation properties of GNSS station in one direction and ignores the spatial correlation between different directions, which cannot accurately reflect the spatio-temporal variation properties of GNSS station. As an extension of SSA, MSSA can simultaneously extract and model multiple time series, and expands the dynamic properties analysis of GNSS station from single-channel to multi-channel (Gruszczynska et al., 2017; Zhou et al., 2020). Compared with SSA, MSSA has better signal extraction and modeling performance. Meanwhile, the mixed signal of colored noise and nonlinear trend signal may present similar form to some useful signal, which may interfere with signal extraction. Xu and Yue (2015) utilized Monte Carlo SSA to detect seasonal oscillation signals of GNSS position time series, and found that SSA-filtered seasonal signals may change the noise properties of original GNSS observations. Klos et al. (2017) utilized different methods to detect the time-varying seasonal signals of GNSS position time series, indicating that the signal extraction results are different under different noise levels. Thus, the influence of colored noise should be considered during the signal extraction and modeling of GNSS position time series.

Considering these problems, MC-MSSA is utilized to simultaneously extract and model the position time series of GNSS station in three directions, which can effectively take into account the spatial correlation of different directions. MC-MSSA distinguishes signal from colored noise through Monte Carlo significance test, which effectively eliminate the interference of colored noise. Then, MC-MSSA is adopted to simultaneously extract and model the tectonic and non-tectonic signals of inter-seismic position time series in three components. Moreover, considering that the eastern Tibetan Plateau is the seismically active region of mainland China, the tectonic signals extracted by MC-MSSA is utilized to characterize the crustal movement and strain rate field, and then reveal the crustal activities during the inter-seismic phase.

2. MONTE CARLO MSSA MODELING SCHEME

2.1. MONTE CARLO MSSA

Multi-channel Singular Spectrum Analysis (MSSA) is an extension of Singular Spectrum

Analysis (SSA). Its main advantage is that it can take into account the coherence between different channels, thus can extract as many signals as possible from the time series and reduce noise interference more effectively (Allen and Robertson, 1996; Ghil et al., 2002; Raynaud et al., 2005). Similar to SSA, MSSA has two major steps: decomposition and reconstruction. Assuming x_{li} is a multi-dimensional time series, l is the number of channels ($l = 1, 2, ...L$), and i is the number of time series per channel ($i = 1, 2, ...N$), the trajectory matrix X of the multi-dimensional time series can be expressed by the following formula (Ghil et al., 2002):

$$X = \begin{bmatrix} x_{11}, x_{12}, \cdots, x_{1i+1}, \cdots, x_{1N-M+1} \\ x_{12}, x_{13}, \cdots, x_{1i+2}, \cdots, x_{1N-M+2} \\ \vdots \\ x_{1M}, x_{1M+1}, \cdots, x_{1i+M}, \cdots, x_{1N} \\ \vdots \\ x_{L1}, x_{L2}, \cdots, x_{Li+1}, \cdots, x_{LN-M+1} \\ x_{L1}, x_{L2}, \cdots, x_{Li+1}, \cdots, x_{LN-M+1} \\ \vdots \\ x_{LM}, x_{LM+1}, \cdots, x_{Li+M}, \cdots, x_{LN} \end{bmatrix} \quad (1)$$

where M indicates the window length. The trajectory matrix X of the multi-dimensional time series has $L*M$ rows and $N-M+1$ columns (Groth and Ghil, 2011). The lag-covariance matrix T_x can be computed by the trajectory matrix X (Kim and Wu, 1999), which can be depicted as：

$$T_x = \begin{bmatrix} T_{11}, T_{12}, \cdots, T_{1L} \\ T_{21}, T_{22}, \cdots, T_{2L} \\ \vdots \\ T_{L1}, T_{L2}, \cdots, T_{LL} \end{bmatrix} \quad (2)$$

where $T_{ll'}$ is the covariance matrix of the time series of channel l and l'. Singular Value Decomposition (SVD) of lag-covariance matrix T_x and diagonalization can obtain the eigenvalues γ_k and eigenvectors E^k of corresponding Spatiotemporal Empirical Orthogonal Functions (ST-EOFs). The eigenpairs (E^k, γ_k) are arranged in descending order according to eigenvalues γ_k, and the ST-EOFs can be utilized to calculate the Spatiotemporal Principal Components (ST-PCs).

$$a_i^k = \sum_{l=1}^{L} \sum_{j=1}^{M} x_{li+j} E_{lj}^k \quad (3)$$

For MSSA, another important step is reconstruction. Based on ST-EOFs and ST-PCs, the Reconstructed Components (RCs) of each time series can be calculated according to the following formula (Plaut and Vautard, 1994):

$$x_{li}^k = \begin{cases} \dfrac{1}{i}\sum\limits_{j=1}^{i} a_{i-j}^k E_{lj}^k, 1 \le i \le M-1 \\ \dfrac{1}{M}\sum\limits_{j=1}^{M} a_{i-j}^k E_{lj}^k, M \le i \le N-M+1 \\ \dfrac{1}{N-i+1}\sum\limits_{j=i-N+M}^{M} a_{i-j}^k E_{lj}^k, N-M+2 \le i \le N \end{cases} \qquad (4)$$

According to the above formula, the different components contained in the time series of each channel can be reconstructed. For each channel, the sum of all components is equal to the original time series. Thus, through the identification and reconstruction of different components, the different geophysical signals contained in GNSS position time series can be extracted and modeled.

When MSSA is utilized to model multi-dimensional position time series, it is a key problem to distinguish signal from noise and select the first k RCs judged as signals for signal reconstruction. Generally, the colored noise in the GNSS position time series may present a similar time-varying pattern to some high-order signals, which may cause some colored noise to be misjudged as signals. Thus, when using MSSA to model GNSS position time series, it is necessary to select appropriate statistical significance test to distinguish signal and colored noise. Considering this problem, this paper utilizes Monte Carlo numerical simulation to conduct significance test for eigenvalues. Allen and Smith (1994) pointed out that the colored noise contained in geophysical time series may interfere with the extraction of useful signals, and adopted Monte Carlo to conduct the significance test for SSA during processing meteorological time series. Since most colored noise in geophysical time series is AR(1), the AR(1) is adopted as the random noise model in this significance test. Compared with some geophysical observations, the colored noise in GNSS position time series is mainly Power Law (PL) noise, which will produce relatively large interference to signal recognition. Thus, the PL noise is regarded as the random noise model of the Monte Carlo significance test in this paper.

The main idea of MC-MSSA modeling is to compare the local variances of analyzed data distributed in the direction defined by ST-EOFs with the corresponding variances generated by the specific null hypothesis (Walwer et al., 2016; Zhang et al., 2017). The null hypothesis of MC-MSSA mainly relies on the construction of a set of surrogate data, which are usually generated based on a specific random noise model. According to the specific random noise model, it is possible to generate surrogate data X_R with the same length N and dimension L of analyzed data. By projecting the covariance matrix $\tilde{T}_R$ of surrogate data to the direction defined by ST-EOFs, the local variance of surrogate data can be calculated:

$$\Lambda_R = E^T \tilde{T}_R E \qquad (5)$$

Among them, the construction method of $\tilde{T}_R$ is similar to that of T_x generated by MSSA, while the $\tilde{T}_R$ is obtained by surrogate data. E^T is the transposed matrix of E, and the $L \times M$ column of E is ST-EOFs E^k. By setting the number of Monte Carlo numerical simulation experiments, using enough surrogate data, a set of data sets of Λ_R can be obtained, and then the confidence interval of the diagonalization elements of Λ_R can be estimated. After that, the eigenvalues of MSSA are compared with the confidence interval of the diagonalization elements of Λ_R. If the eigenvalue is within or below the confidence interval, indicating that the corresponding component is indistinguishable from the surrogate data generated by the noise model, which can be judged as noise. Conversely, if the eigenvalue is outside or above the confidence interval, the null hypothesis is rejected, indicating that its corresponding component and the surrogate data generated by the noise model have different statistical meanings, which can be judged as useful signal.

2.2. KENDALL NONPARAMETRIC TEST

Vautard et al. (1992) pointed out that the trend components in the time series usually appears in the first few RCs, and the Kendall nonparametric test is an effective method to identify the trend components. Since the research object of this paper is multi-channel time series, this method can be utilized to distinguish the RCs of the time series of each channel. Z_i^l indicates the time series of group l, where i is the length of time series ($1 \le i \le n$), l is the number of channel ($1 \le l \le L$). For the time series Z_i^l, we statistics the logarithm of index (i,j) which satisfies $i < j, Z_i^l < Z_j^l$ (i and j are not necessarily adjacent). In general, large K_r^l indicates that there is an upward trend component in the time series, while small K_r^l denotes that there is a downward trend component. The quantitative test of this method is mainly based on the following statistics:

$$\tau^l = \frac{4K_r^l}{n(n-1)} - 1 \qquad (6)$$

When the hypothesis that there are no trend components in the detected time series Z_i^l is established, it satisfies a normal distribution with the mean value of 0 and the variance of:

$$s^l = \sqrt{\frac{2(2n+5)}{9n(n-1)}} \qquad (7)$$

When τ^l is outside the interval $(-1.96s^l, 1.96s^l)$ (the reliability is assumed to be 0.05), the null hypothesis

is rejected, indicating that there are trend components in the time series. When $\tau^l > 1.96s^l$ and $\tau^l < -1.96s^l$, it means that the time series has the upward and downward trend components, respectively. The trend components in the time series can be obtained by adding the detected trend components, while the sum of other reconstructed components is the detrended time series. The above process is iteratively iterated until there is no trend component in the RCs and the detection is finished.

2.3. W-CORRELATION COEFFICIENT

For the GNSS position time series, the periodic oscillation signal is an important part, which is mainly manifested in the form of annual and semi-annual changes. Plaut and Vautard (1994) pointed out that the following three principles can be used to identify periodic signals: 1) two consecutive eigenvalues are almost equal, and the variance corresponding to the eigenvalues are almost equal; 2) the corresponding ST-EOFs are orthogonal and have similar periodic changes; 3) The corresponding ST-PCs are also orthogonal. For the significant annual and semi-annual signals in GNSS position time series, the above mentioned criteria is an effective identification method. However, due to the influence of local environment, there will be some other insignificant periodic signals in the position time series, which is difficult to be distinguished by this method. Hassani et al. (2007) utilized the W-correlation method to identify periodic oscillation signals, which can effectively identify the insignificant periodic signals in some time series in comparison with the above methods. Assuming x_i is a set of time series ($i = 1, 2, \ldots, L$) and Y_i is its reconstruction component, the W-correlation coefficients of any two RCs can be expressed by the following formula:

$$\rho_{i,j}^w = \frac{(Y^{(i)}, Y^{(j)})}{\|Y^i\|_w \|Y^j\|_w} \tag{8}$$

Among them, $\|Y^i\|_w = \sqrt{(Y^{(i)}, Y^{(i)})}$,

$(Y^{(i)}, Y^{(j)}) = \sum_{k=1}^{N} w_k y_k^i y_k^j$, $w_k = \min(k, M, n-k)$. The

larger the value of $\rho_{i,j}^w$, the greater the correlation between the two corresponding RCs, which can be classified as a group of periodic signals. Thus, this paper mainly combines the two methods to identify the periodic signals of GNSS position time series.

3. RESULTS AND DISCUSSION
3.1. COMPARISON OF MSSA AND SSA

Compared with SSA, MSSA can extract as much signal as possible from GNSS position time series by taking into account the correlation between different channels. Considering that many studies have compared SSA with traditional methods, this paper only discusses the performance of SSA and MSSA on

signal extraction and modeling. Due to the effect of tectonic movement, the horizontal components of GNSS position time series have significant trend signals. If SSA and MSSA are utilized to model the horizontal components of GNSS position time series separately, the difference cannot be clearly observed in detail. Thus, in order to make the comparison more obvious, the SSA and MSSA are utilized to extract and model the vertical component of GNSS coordinate time series. Taking the station XIAG of the Crustal Movement Observation Network of China (CMONOC) as an example (the time span is 2012.0014–2017.0014), the vertical component of GNSS position time series is modeled by SSA. Meanwhile, the MSSA is used to simultaneously model the vertical components of the GNSS position time series of station XIAG and its nearest station KMIN. When using SSA and MSSA to model GNSS position time series, a key issue is the selection of lag-window size. Some studies suggest that the 2-year window may be more suitable for the extraction of seasonal signals, and can obtain higher spectral resolution (Ghil et al., 2002; Rangelova et al., 2012; Li et al., 2017a; Xiang et al., 2019). Thus, the lag-window size is chosen as 2 years in order to extract and model the signal more accurately.

Then, the two methods are utilized to model the vertical component of GNSS position time series of station XIAG, and Figure 1 shows the regularized eigenvalues generated by SSA and MSSA and the variance percentage of first 10 RCs. For the vertical GNSS position time series of station XIAG, among the first 10 RCs, RC1 and RC2 represent the annual signal, RC3 and RC4 represent the semi-annual signal, RC5 and RC6 represent the nonlinear trend, and RC7–10 represent other signals. For SSA, the variance percentages of the annual, semi-annual, and nonlinear trend signals are 43 %, 5 %, and 4 %, respectively. As for MSSA, the variance percentages of the annual, semi-annual, and nonlinear trend signals are 51 %, 6 %, and 4 %, respectively. It can be seen that there is significant annual signal in the vertical GNSS position time series of station XIAG, followed by semi-annual and nonlinear trend signals. The variance percentage of the three signals extracted by MSSA is 61 %, which is 9 % higher than the variance percentage of the three signals extracted by SSA (i.e., 52 %), indicating that MSSA can extract as much signal as possible from noisy GNSS position time series and minimize the interference of colored noise.

In general, the first 10 RCs basically contain the main signals of GNSS position time series. In order to further discuss the performance of SSA and MSSA on signal extraction and modeling, the first 10 RCs obtained by two methods are added respectively (Fig. 2). The SSA-modeled signal has obvious fluctuations in the details, while the MSSA-modeled signal is relatively smooth. It can be seen that the SSA-modeled signal is more susceptible to noise interference, and the modeled signal contains more noise that cannot be identified by SSA. MSSA can
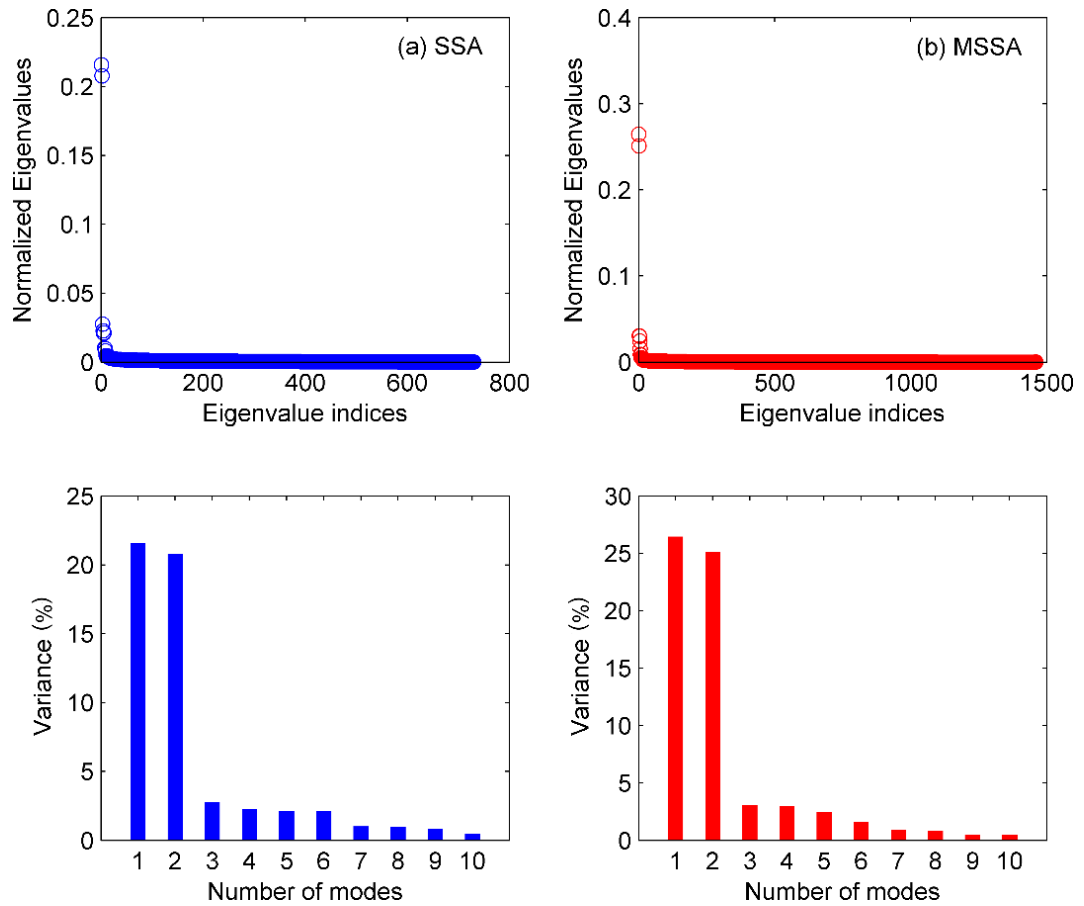
Fig. 1 Normalized eigenvalues and variance percentage of the first 10 RCs generated by SSA (a) for station XIAG the and MSSA (b) for stations XIAG and KMIN.
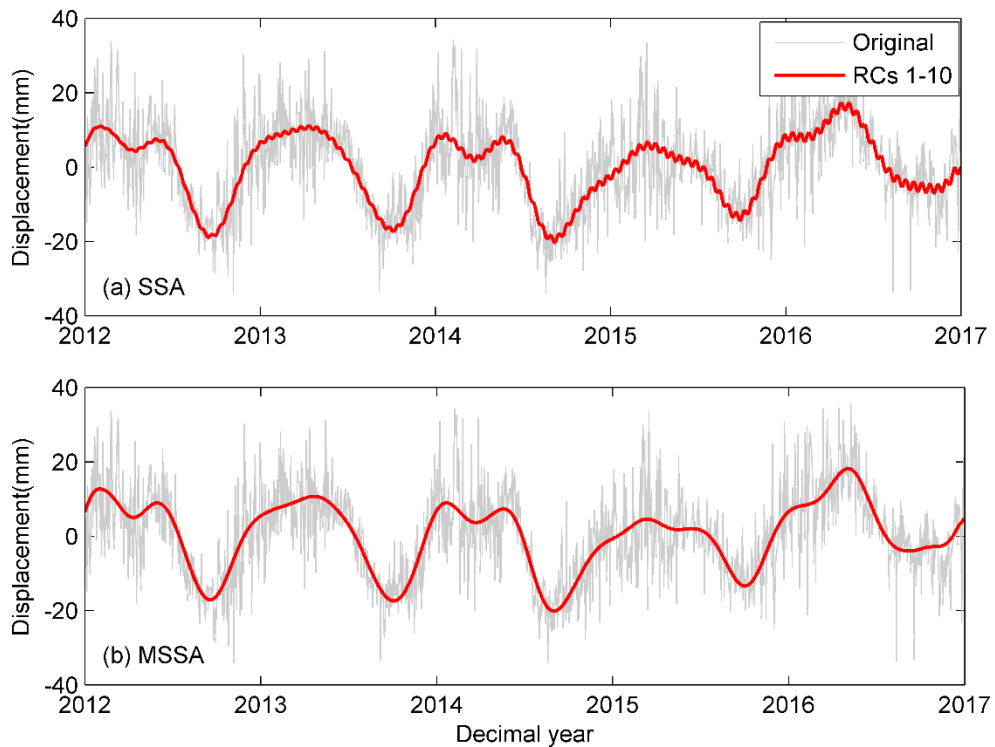
Fig. 2 Comparison of the signals modeled by SSA (a) and MSSA (b) for the vertical GNSS position time series of station XIAG.
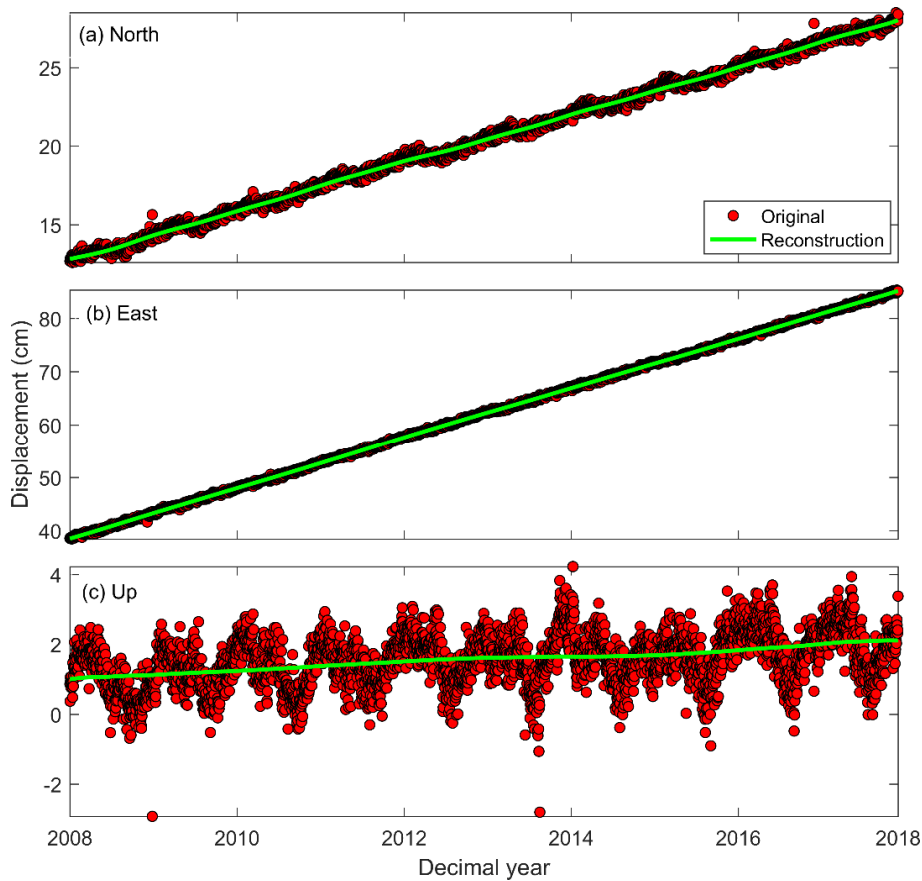
Fig. 3 Modeled trend signals and original GNSS position time series of station LHAZ in the three components.

distinguish these noise that cannot be identified by SSA by taking into account the correlation of different channels, and thus it has better signal extraction performance. The result denotes that MSSA has better signal extraction and modeling performance by taking into account the correlation of different channels in comparison with SSA. In addition, MSSA can simultaneously process multi-channel time series, which has higher processing efficiency.

3.2. GNSS POSITION TIME SERIES MODELING SCHEME

Taking the station LHAZ derived from the International Ground Station (IGS) network as an example, MC-MSSA is utilized to simultaneously model the different signals of the position time series in the three components. The time span of the position time series of station LHAZ is 2008.0014–2018.0014, which is provided by Scripps Orbit and Permanent Array Center (SOPAC). Its horizontal components contain obvious trend components, and the periodic variation components exist in the three components. Chen et al. (2013) suggested that a lag-window size of 2 years is suitable to extract seasonal signals from GNSS position time series. Considering the significant signals in the three components, the lag-window of MSSA is selected as 2 years in order to extract different signals more accurately. MSSA is utilized to

decompose and reconstruct the three components of the position time series of station LHAZ at the same time. After that, Kendall non-parametric test is carried out for the first few RCs of each channel to identify the trend components. The first 2 RCs of each channel are identified as trend components, where RC1 and RC2 are linear and nonlinear trend components respectively. Then, RC1 and RC2 of each channel is added to obtain the trend components of the position time series of each channel (Fig. 3), and there are significant trend signals in the horizontal components in comparison with the vertical component.

For the GNSS position time series, it not only includes the trend signals caused by tectonic movements, but also includes the periodic signals caused by geophysical factors (e.g., surface mass loading), white noise, and colored noise. In general, the extraction of periodic signals can be disturbed by the colored noise in the GNSS position time series. Therefore, how to distinguish multiscale periodic signals from colored noise, and then extract periodic signals from the position time series is a key issue. MSSA is utilized to decompose and reconstruct the detrended GNSS position time series, and W-correlation analysis is carried out for the reconstructed RCs (Fig. 4). It can be seen that every two adjacent RCs of the first 10 RCs have a strong correlation, the W-correlation coefficient is close to 1,
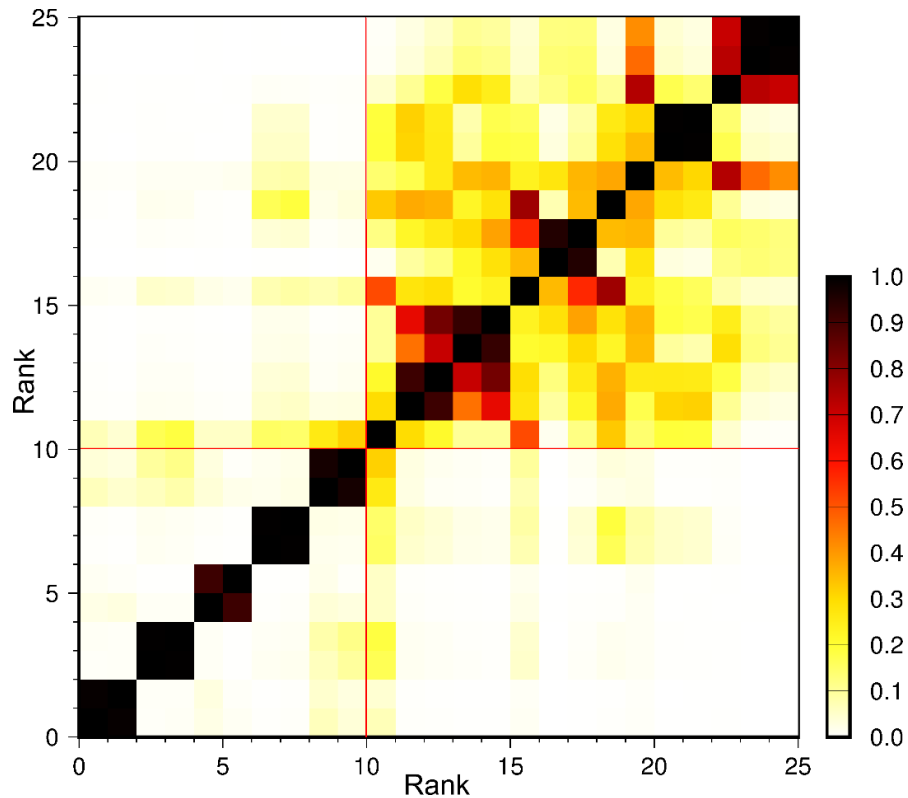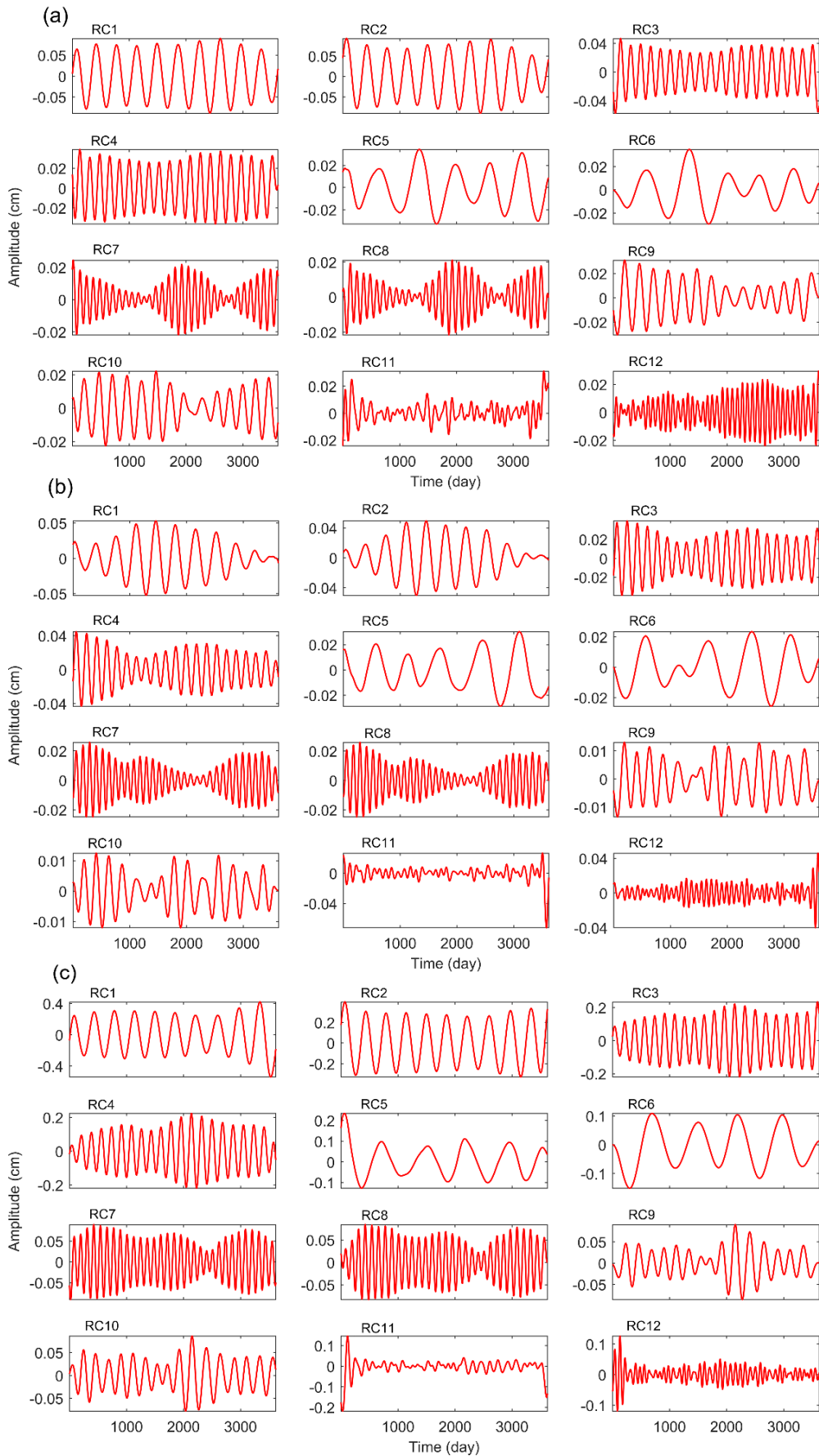
Fig. 4   W-correlation analysis result of the first 25 RCs generated by MSSA.

and the correlation with other high-order RCs is close to 0. For the RCs with rank greater than 10, there is no strong correlation between adjacent RCs. Meanwhile, there is also a certain correlation between RCs with rank greater than 10 and higher-order RCs, indicating that the RCs with rank greater than 10 cannot be well distinguished from noise. According to the identification criterion of periodic signal, the larger coefficient indicates the larger the correlation between the two RCs, which can be classified as a group of periodic signals. Thus, the first 10 RCs are considered as periodic signals, and RC1–2, RC3–4, RC5–6, RC7–8 and RC9–10 can be regarded as different periodic signals.

Figures 5a–c show the first 12 RCs of the three components of the position time series of station LHAZ, and Figures 6a–c depict the Fast Fourier Transform (FFT) detection results of the first 12 RCs of the three components. It can be seen that the first 10 RCs have obvious periodic changes, and the adjacent RCs present similar periodic changes. When the rank of RCs is greater than 10, the RCs of three channels present an irregular oscillation change, and the changes of RC11 and RC12 are not similar. The result also indicates that the first 10 RCs are periodic signals, while no paired periodic changes occur since RC11, which is more likely to be noise. This is consistent with the result of W-correlation analysis. After that, FFT analysis is utilized to detect the period of the RCs of each channel, and every adjacent RCs of the first 10 RCs appears same period, which can be regarded as a group of periodic signals. The first

10 RCs of the position time series of each channel contain 5 kinds of periodic signals: 1) the period of RC1+RC2 is 1 cpy (cycle per year) (i.e., annual term); 2) the period of RC3+RC4 cycle is 2 cpy (i.e., semi-annual term); 3) the period of RC5+RC6 cycle is 0.5 cpy; 4) the period of RC7+RC8 cycle is 3 cpy; 5) the period of RC9+RC10 cycle is 1.5 cpy.

Notably, some mixed signals of colored noise and trend terms may show a similar form to some signals, which can be misjudged as useful signals by the above methods. Previous studies indicate that the mixed signal of colored noise and trend component can easily pass the pairwise identification criterion of periodic signals. Therefore, it is not rigorous to use only the pairwise identification criterion and W-correlation to distinguish signal and noise. Considering this problem, Monte Carlo numerical simulation is adopted to conduct the significance test for the eigenvalues generated by MSSA. Since the colored noise in the GNSS position time series is mainly PL noise, the PL noise is regarded as the random noise model of MC-MSSA. The corresponding surrogate data is generated by combining the lag-covariance matrix $\tilde{T}_R$ and ST-EOFs, and the 95 % confidence interval is generated by 500 Monte Carlo tests. Then, the eigenvalues of lag-covariance matrix are compared with the confidence interval of significance test. When the eigenvalue is outside the confidence interval, indicating that the null hypothesis is rejected, and the corresponding RCs is not interfered by colored noise. Conversely, when the eigenvalue is within the
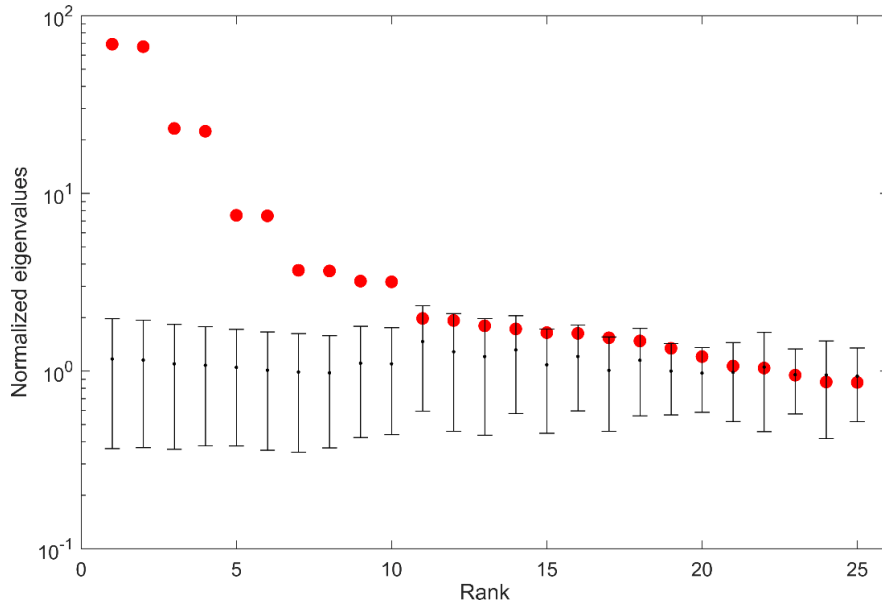
Fig. 5	The first 12 RCs of the GNSS position time series of station LHAZ in the north (a), east (b), and up (c) component.
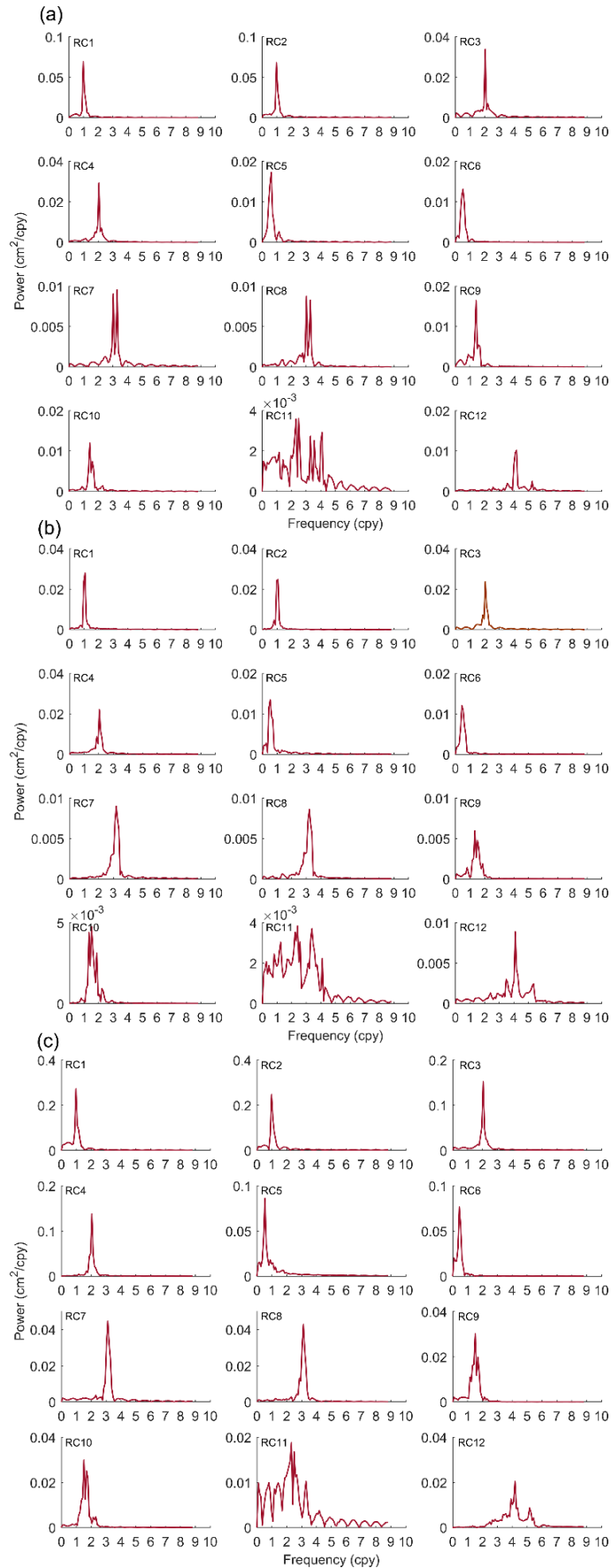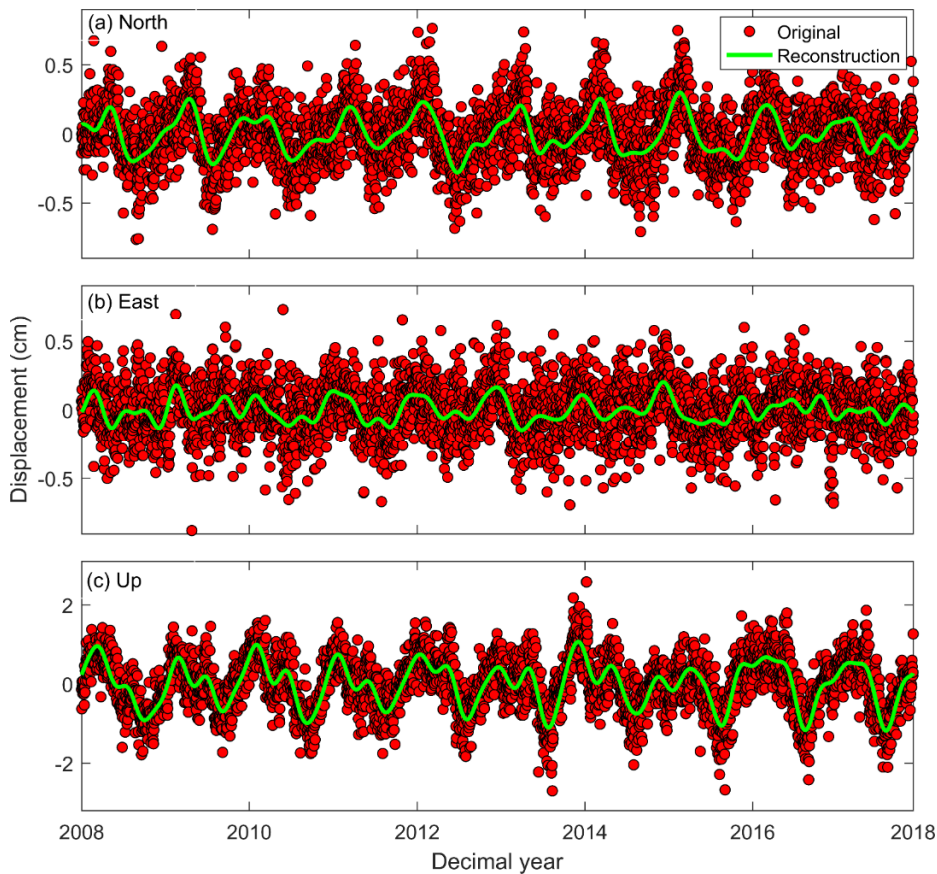
Fig. 6 FFT analysis result of the first 12 RCs of the GNSS position time series of station LHAZ in the north (a), east (b), and up (c) component.

Fig. 7   The result of 95 % Monte Carlo significance test for first 25 ranks, and the error bars represent the confidence interval of the significance test.

Fig. 8   Modeled seasonal signals and the detrended GNSS position time series of station LHAZ in the three components.

confidence interval, suggesting that the RCs corresponding to the eigenvalues is noise. As depicted in Figure 7, the first 10 eigenvalues are all outside the confidence interval, rejecting the null hypothesis, and indicating that the RCs corresponding to first 10 eigenvalues are useful signals, which have certain geophysical significance. Starting from the 10th eigenvalue, the eigenvalue starts to be within the confidence interval, indicating that RCs with the rank greater than 10 are noise. Therefore, the first 10 RCs in each channel are utilized to reconstruct the signal of the detrended position time series (Fig. 8).
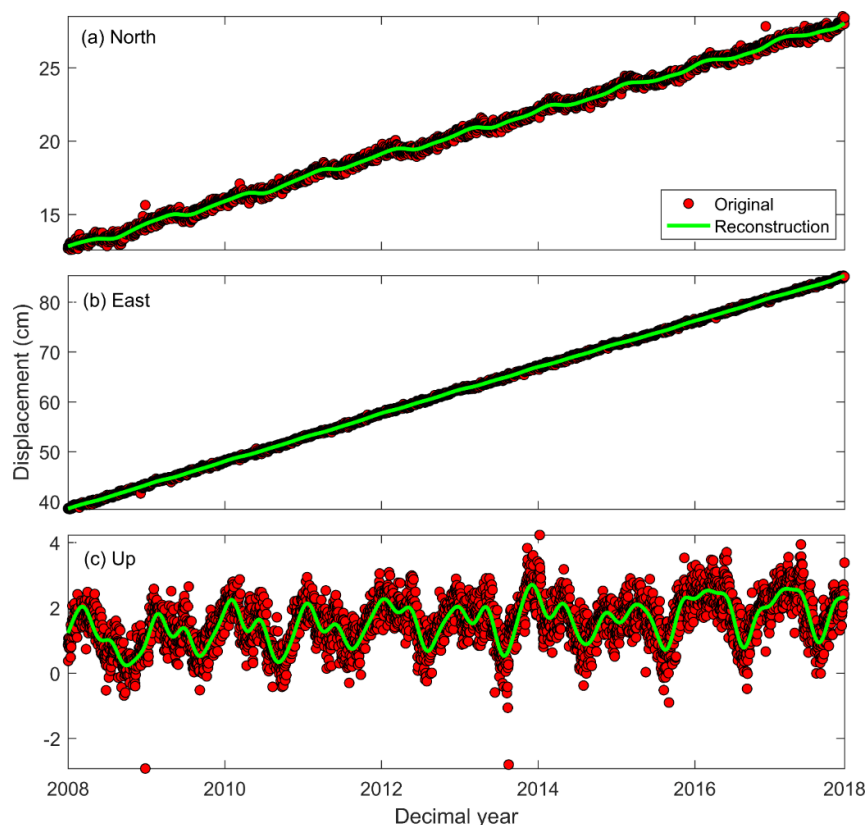
Fig. 9   Modeled signals and original position time series of station LHAZ in the three components.

The tectonic and non-tectonic signals can be reconstructed by adding all RCs identified as signals. The signals modeled by MC-MSSA greatly reduces the noise level of GNSS position time series, and can clearly describe the tectonic and non-tectonic signals (Fig. 9). The RMS values of the GNSS position time series in the N, E, and U components are decreased by 1.79, 1.81, and 4.45 mm, respectively. Meanwhile, the MC-MSSA-modeled signals can more intuitively reflect the three-dimensional dynamic changes of this station (Fig. 10). In the horizontal components, the station has clear trend movement toward the northeast during 2008–2018 with a certain amount of seasonal oscillation movement. In the vertical component, the station appears significant seasonal oscillation movement with a certain uplift trend. According the extracted trend components, the GNSS velocity of this station can be estimated, and the movement rates in the N, E, and U components are 46.6, 15.3, and 1.2 mm/a, respectively. The above results denote that MC-MSSA can effectively extract and model the tectonic and non-tectonic signals of inter-seismic GNSS position time series, which can more intuitively reflect the dynamic movement of the station. Moreover, MC-MSSA can take into account the spatial correlation between different components by simultaneously modeling GNSS position time series in three components, and can effectively distinguished the signal and colored noise through the significance test.

3.3. *APPLICATION TO DETERMINING CRUSTAL DEFORMATIONS IN EASTERN TIBETAN PLATEAU*

The Tibetan Plateau is located at the edge of the Indian and Eurasian plate. Due to the collision between the two plates, the geological structure of this region is complex and the crustal tectonic movement is active (Li et al., 2008; Copley et al., 2011; Styron et al., 2015). Meanwhile, the eastern Tibetan Plateau spans several provinces, and the junction with the Sichuan Basin is the Longmenshan fault zone, which is one of the most seismically active regions in mainland China. Thus, characterizing the crustal deformations in eastern Tibetan Plateau is of great significance for seismically risk assessment in mainland China.

In order to characterize the crustal motion properties of eastern Tibetan Plateau, the GNSS observations of 30 stations derived from CMONOC are selected, and the time span is 2011.0014–2016.0014. The GNSS position time series are provided by the GNSS data product service platform of China Earthquake Administration. More details about data processing can refer to ftp://ftp.cgps.ac.cn/doc/processing_manual.pdf. The MC-MSSA is adopted to simultaneously extract the signals of the three components of each GNSS position time series, and the GNSS velocity under the ITRF14 framework is estimated using modeled trend
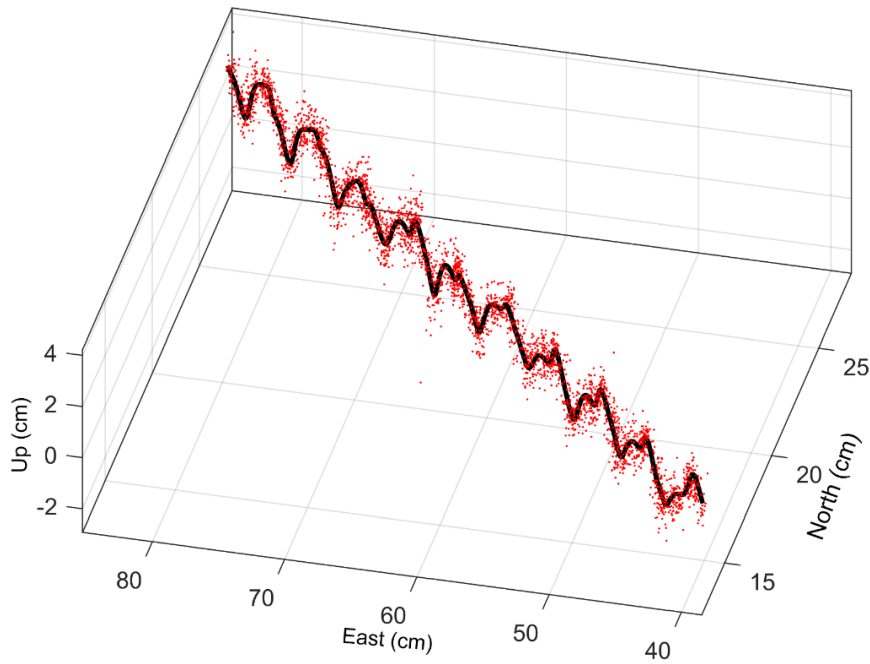
Fig. 10 Three-dimensional dynamic change of station LHAZ during the time span of 2008.0014–2018.0014.

signals. In this paper, we mainly utilize horizontal GNSS velocity to characterize crustal movements and strain rate changes in eastern Tibetan Plateau. Meanwhile, the modeled seasonal signals of GNSS position time series in the vertical component are adopted to explore non-tectonic crustal deformations.

(a) Regional crustal movement

As exhibited in Figure 11, the movement rates of all stations in the EW direction are significantly greater than that in the NS direction. The magnitude of velocity rate in the EW direction is [30 50] mm/a, while it is [–20 5] mm/a in the NS direction. The junction of eastern Tibetan Plateau and Sichuan Basin is the Longmenshan fault zone. The peak region of GNSS velocity is focused on the left side of the Longmenshan fault zone, and the velocity rates in the EW direction are all above 40 mm/a (the maximum reaches 49.2 mm/a at station XZCD). On the right side of Longmenshan fault zone, the velocity rates are significantly reduced, which vary from 33.9 to 36.9 mm/a in the EW direction. Meanwhile, the velocity rates outside the Tibetan Plateau in the Yunnan and Sichuan provinces that belong to the South China block are also significantly reduced. The above results indicate that compared with South China block, the GNSS velocity rates in the Tibetan Plateau are significantly higher, implying that the tectonic activity in the Tibetan Plateau is stronger. The main reason for this phenomenon is that the movement of Tibetan Plateau induced by the pushing of Indian plate is blocked by South China block, and the crustal movement rates are obviously decreased, which appear a clockwise movement trend.

(b) Crustal strain rate changes

In order to explore the crustal dynamic mechanism of eastern Tibetan Plateau, the strain rate changes are estimated based on GNSS velocities. It can be seen from Figure 12 that the principal strain rates in the South China block are relatively small, and the amplitudes are within 10 nanostrain/yr (i.e., 10^{-8} /yr), indicating that the interior of the block is relatively stable. The principal strain rates inside the Tibetan Plateau are obviously greater than other regions, and the amplitude of extension stress rate is larger than compression stress rate, indicating that the push-squeeze force from the Indian plate has caused tensile deformations inside the Tibetan Plateau. The junction of southeastern Tibetan Plateau and South China block appear principal compression stress rate, especially in the Longmenshan fault zone. The maximum of principal compression stress rate amplitude is –93.9 nanostrain/yr. The results indicate that since the crustal movement of Tibetan Plateau is blocked by the South China block, the junction of the Tibetan Plateau and South China block produces a certain compression stress.

The dilatational strain rate ranges from –77.2 to 50.2 nanostrain/yr with average of –3.0 nanostrain/yr. The dilatational strain rate inside the Tibetan Plateau is positive, implying that the crust inside the Tibetan Plateau has undergone expansion deformation, which is consistent with the result of principal strain rate analysis. The largest dilatational strain rate (reaching 50.2 nanostrain/yr) is located at the junction of southeastern Tibetan Plateau and South China block. The negative dilatational strain rate is mainly concentrated in two regions, namely Sichuan Basin
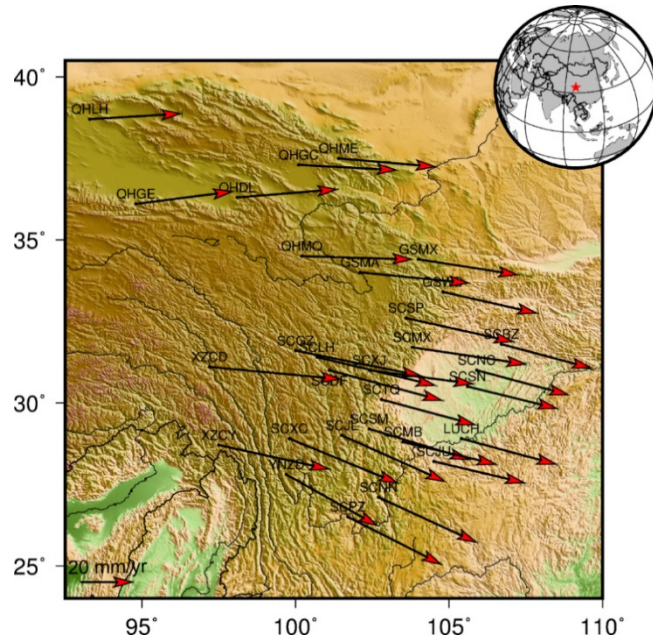
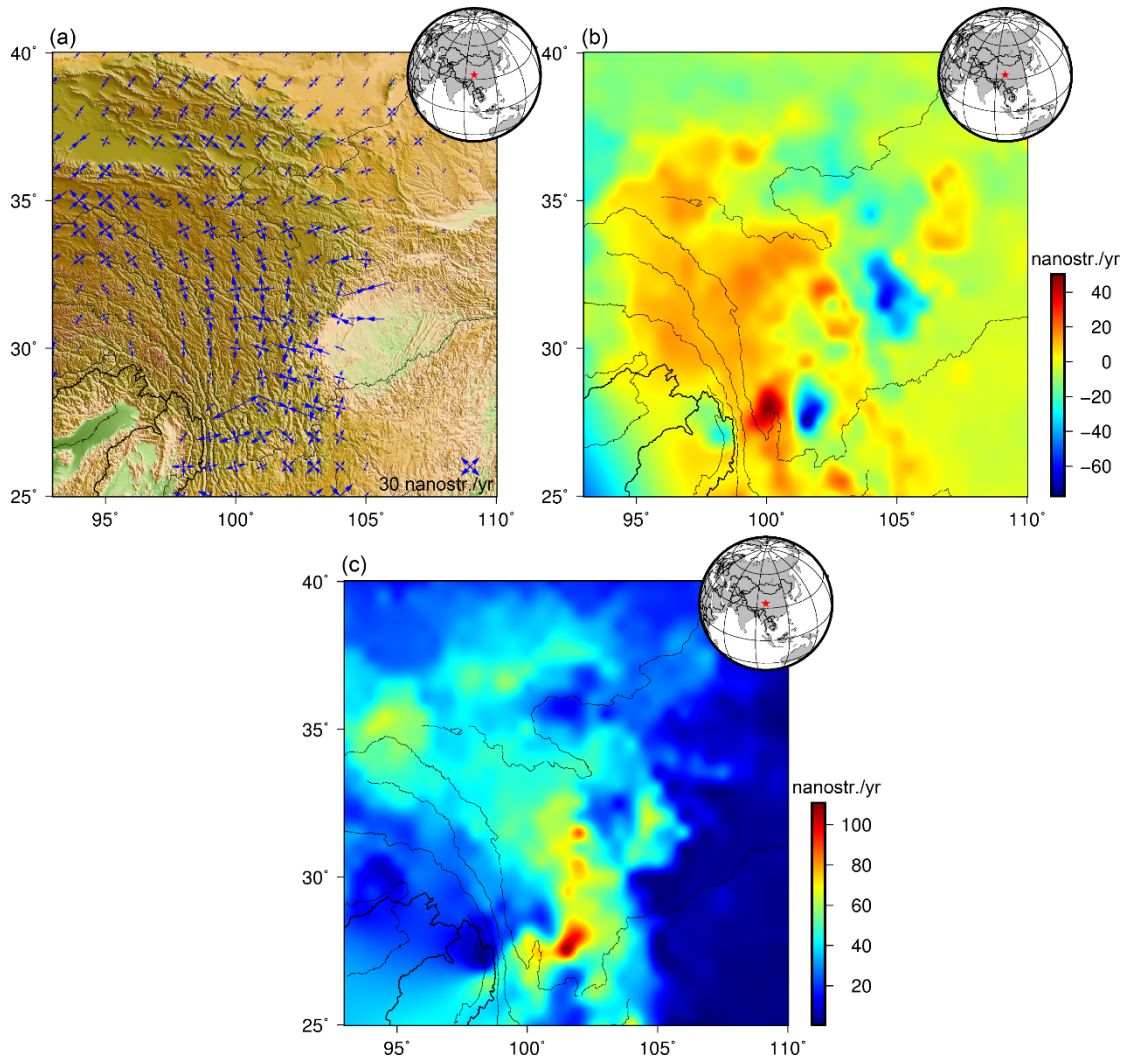**Fig. 11** GNSS velocity of 30 stations in the eastern Tibetan Plateau.
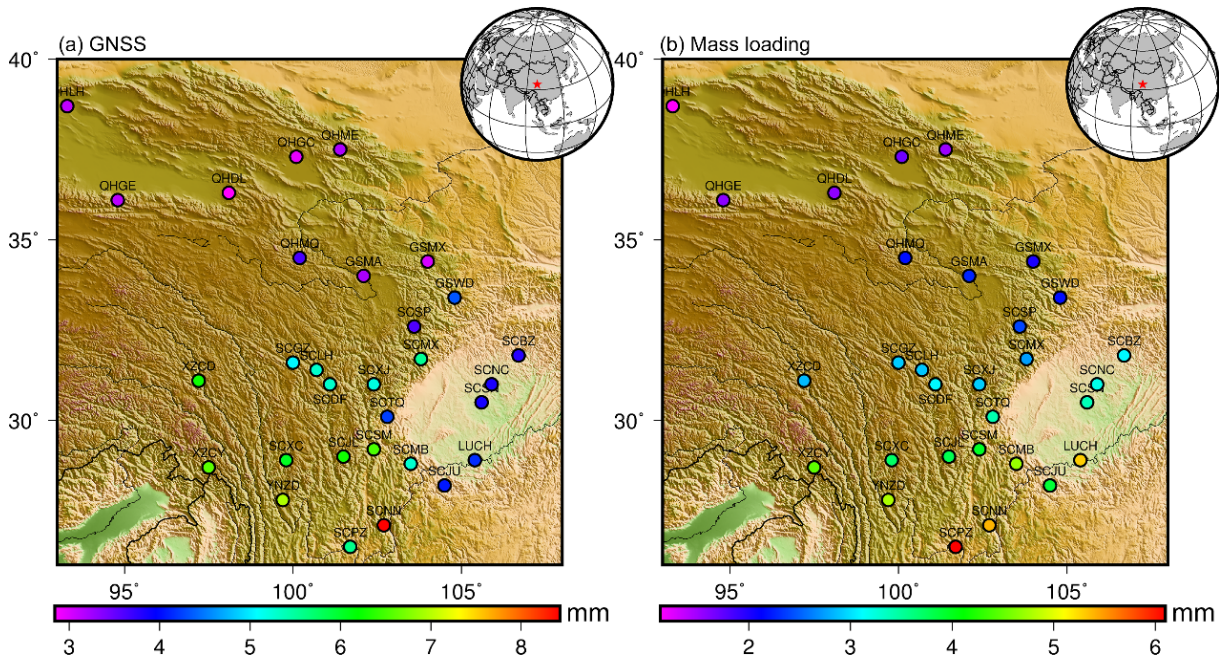

Fig. 12 Spatial distribution of the principal strain rate, dilatational strain rate, and maximum shear strain rate over the eastern Tibetan Plateau.

Fig. 13 Spatial distribution of the RMS values of vertical GNSS position timing series (a) and surface mass load deformations (b) at 30 stations.

and Yunnan province. The minimum of dilatational strain rate is –77.2 nanostrain/yr, which is located in Sichuan province. The result suggests that the interior of Tibetan Plateau is dominated by expansion deformation, and the collision between Tibetan Plateau and South China block results in the shrinkage deformation in the junctions, which is particularly prominent in the Sichuan Basin.

The maximum shear strain rate varies from 0.1 to 110.8 nanostrain/yr with average of 27.8 nanostrain/yr. It can be seen that the larger values of maximum shear strain rate are concentrated in the interior of the Tibetan Plateau and the junction of eastern Tibetan Plateau and southern China block. The maximum shear strain rate of other regions in the Tibetan Plateau is below 20 nanostrain/yr, and the maximum shear strain rate inside the South China block is close to 0 nanostain/yr. The peak of maximum shear strain rate is located at the junction of Tibetan Plateau and South China block in the Sichuan-Yunnan region, and the maximum reaches 110.8 nanostrain/yr. The second is the Longmenshan fault zone (i.e., the junction of eastern Tibetan Plateau and Sichuan Basin), which are above 70 nanostrain/yr. The above results indicate that the junction of Tibetan Plateau and South China block has accumulated a certain amount of stress due to the fact that the crustal movement of Tibetan Plateau is blocked by the South China block. The crustal tectonic activity at the junction is relatively strong, which still belongs to the dangerous zone of seismic activity.

(c) Non-tectonic crustal deformations

Considering that seasonal oscillations are an important part of GNSS position time series, this paper

also briefly discusses the non-tectonic crustal deformations in the eastern Tibetan Plateau using MC-MSSA-modeled seasonal signals. We adopt the global loading grids with the spatial resolution of $0.5^{\circ} \times 0.5^{\circ}$ provided by the German GeoForschungs Zentrum (GFZ) to estimate deformations induced by mass loading. The time resolution of atmospheric, non-ocean tidal loading, and hydrological loading is 3, 3, and 24 h, respectively.

To a certain extent, the Root Mean Square (RMS) value of GNSS position time series and surface mass loading deformations can reflect the dispersion degree and amplitude of seasonal fluctuations, and then can reflect the effect of non-tectonic crustal deformations. It can be seen from Figure 13 that the spatial distribution of the RMS values of two displacement time series presents strong latitude dependence. The high RMS values are concentrated in the low latitude areas of eastern Tibetan Plateau (i.e., Sichuan and Yunnan provinces), while the low RMS values is focused on the high latitude areas (i.e., Qinghai and Gansu provinces).

Previous studies have proved that both the vertical GNSS position time series and surface mass loading deformations have significant annual signals, and surface mass loading mainly affects the annual change of GNSS position time series (Ray et al., 2008; Xu, 2016; Xu, 2017). Thus, this paper mainly focuses on the annual signals of two displacement time series. Figure 14 shows the comparison of the annual signals of vertical GNSS position time series and surface mass loading deformations. Among them, 3 stations QHDL, QHGC, and QHMQ are located in Qinghai Province (i.e., high latitude areas), 2 stations GSMA and GSWD are located in Shaanxi Province (i.e., mid-latitude
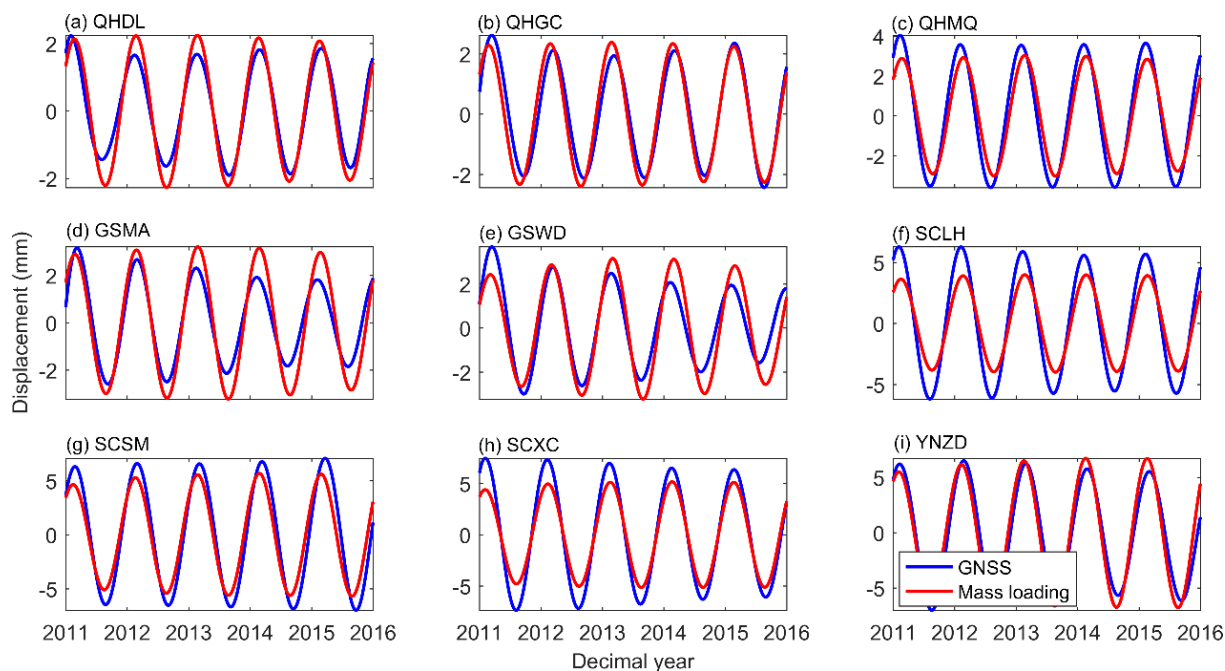
Fig. 14 Comparison of the annual signals of vertical GNSS position time series and surface mass loading deformations.

areas), and 4 stations SCLH, SCXC, SCXJ, and YNZD are situated in Sichuan and Yunnan provinces (i.e., low latitude areas). The annual signal amplitudes of two displacement time series at 4 stations in low latitude areas is significantly larger than other areas, indicating that the effect of surface mass loading is more significant as the latitude decreases. For stations QHGC and YNZD, two annual signals have a high consistency in terms of amplitude and phase, indicating that surface mass loading is the dominant factor of the annual oscillation in GNSS position time series. For most stations, the phases of two annual signals are relatively consistent, while the amplitudes are different, demonstrating that surface mass loading can only partly explain the annual oscillations of GNSS position time series. For few stations, two annual signals have large differences in amplitude and phase, implying that surface mass loading cannot explain the annual oscillations of GNSS position time series. The above results demonstrate that the surface mass loading effects in the eastern Tibetan Plateau display strong latitude dependence, and becomes more significant as the latitude decreases. Meanwhile, for most stations, the surface mass loading cannot fully explain the seasonal fluctuations in GNSS position time series. Other geophysical factors (e.g., expansion and contraction of the earth, changes in groundwater reserves, high-order ionospheric disturbances, and thermal expansion and contraction of observation piers), unmodeled system errors (e.g., satellite orbit errors and multipath effects), and surface mass loading jointly causes the annual fluctuations of vertical GNSS position time series (Fu et al., 2013; Li et al., 2017; Xu, 2016; Xu, 2017).

4. CONCLUSION

In general, the GNSS position time series modeling method may ignore the correlation between different directions of the station. Considering this problem, a set of signal extraction and modeling scheme based on MC-MSSA is proposed in this paper, which can simultaneously extract and model the three components of GNSS position time series, and adopts Monte Carlo significance test to distinguish signal from colored noise. Firstly, taking the position time series of station XIAG as an example, the performance of SSA and MSSA on signal extraction and modeling is evaluated. After that, taking station LHAZ as an example, the MC-MSSA is used to simultaneously extract and model tectonic and non-tectonic signals of GNSS position time series in three components, and the Monte Carlo significance test is utilized to identify signal from colored noise. At last, taking the eastern Tibetan Plateau as the research region, the tectonic signals recorded by GNSS stations around the eastern Tibetan Plateau are extracted and modeled using MC-MSSA. Based on the extracted tectonic signals, we explore the crustal movement and strain rate change in the eastern Tibetan Plateau, and then reveals the properties of tectonic activity. In addition, we also briefly discuss the non-tectonic deformations induced by surface mass loading in this region according to modeled seasonal signals.

REFERENCES

Allen, M.R. and Smith, L.A.: 1994, Investigating the origins and significance of low-frequency modes of climate variability. Geophys. Res. Lett., 21, 10, 883–886.

Allen, M.R. and Robertson, A.: 1996, Distinguishing modulated oscillations from colored noise in multivariate datasets. Clim. Dyn., 12, 11, 775–784. DOI: 10.1007/s003820050142

Altamimi, Z., Collilieux, X. and Métivier, L.: 2011, ITRF2008: an improved solution of the international terrestrial reference frame. J. Geod., 85, 8, 457–472. DOI: 10.1007/s00190-011-0444-4

Blewitt, G., Lavalle, D., Clarke, P. and Nurudinov, K.: 2001, A new global model of Earth deformation: seasonal cycle detected. Science, 294, 2342–2345. DOI: 10.1126/science.1065328

Bock, Y., Kedar, S., Moore, A.W., Fang, P. et al.: 2016, Twenty-two years of combined GPS products for geophysical applications and a decade of seismogeodesy. International Association of Geodesy Symposia, Springer, 1-6. DOI: 10.1007/1345_2016_220

Copley, A., Avouac, J.P. and Wernicke, B.P.: 2011, Evidence for mechanical coupling and strong Indian lower crust beneath southern Tibet. Nature, 472, 7341, 79–81. DOI: 10.1038/nature09926

Chen, Q., Dam, T.V., Sneeuw, N., Collilieux, X., Weigelt, M. and Rebischung, P.: 2013, Singular spectrum analysis for modeling seasonal signals from GPS time series. J. Geodyn., 72, 12, 25–35. DOI: 10.1016/j.jog.2013.05.005

Davis, J.L., Wernicke, B.P. and Tamisiea, M.E.: 2012, On seasonal signals in geodetic time series. J. Geophys. Res., Solid Earth, 117(B1), B01403. DOI:10.1029/ 2011JB008690

Dietrich, R., Dach, R., Engelhardt, G., Ihde, J., Korth, W., Kutterer, H.J. et al.: 2001, ITRF coordinates and plate velocities from repeated GPS campaigns in Antarctica - An analysis based on different individual solutions. J. Geod., 74, 11-12, 756–766. DOI: 10.1007/s001900000147

Elliott, J.R., Walters, R.J. and Wright, T.J.: 2016, The role of space-based observation in understanding and responding to active tectonics and earthquakes. Nat. Commun., 7, 13844. DOI: 10.1038/ncomms13844

Feigl, K.L. and Thatcher, W.: 2006, Geodetic observations of post-seismic transients in the context of the earthquake deformation cycle. CR Geosci., 338, 14-15, 1012–1028. DOI: 10.1016/j.crte.2006.06.006

Fu, Y., Argus, D.F., Freymueller, J.T. and Heflin, M.B.: 2013, Horizontal motion in elastic response to seasonal loading of rain water in the Amazon Basin and monsoon water in Southeast Asia observed by GPS and inferred from GRACE. Geophys. Res. Lett., 40, 6048–6053. DOI: 10.1002/2013GL058093

Ghil, M., Allen, M.R., Dettinger, M.D., Ide, K., Kondrashov, D., Mann, M.E., Robertson, A.W., Saunders, A., Tian, Y., Varadi, F. and Yiou, P.: 2002, Advanced spectral methods for climatic time series. Rev. Geophys., 40, 1, 1–41. DOI: 10.1029/2001RG000092

Groth, A., and Ghil, M.: 2011, Multivariate singular spectrum analysis and the road to phase synchronization. Phys. Rev. E, 84, 3, 036206. DOI: 10.1103/PhysRevE.84.036206

Gruszczynska, M., Klos, A., Rosat, S. and Bogusz, J.: 2016, Investigation of time-changeable seasonal components in GPS height time series: A case study for Central Europe. Acta Geodyn. Geomater., 13, 3(183), 281–289. DOI: 10.13168/AGG.2016.0010.

Hassani, H.: 2007, Singular spectrum analysis: Methodology and comparison. J. Data Sci., 5, 2, 239–257. DOI: 10.6339/JDS.2007.05(2).396

He, X., Montillet, J.P., Fernandes, R., Bos, M., Yu, K., Hua, X. and W. Jiang: 2017, Review of current GPS methodologies for producing accurate time series and their error sources. J. Geodyn., 106, 12–29. DOI: 10.1016/j.jog.2017.01.004

He, X., Yu, K., Montillet, J.P., Xiong, C., Lu, T., Zhou, S., Ma, X., Cui, H. and Ming, F: 2020, GNSS-TS-NRS: An Open-source MATLAB-based GNSS time series noise reduction software. Remote. Sens., 12, 21, 3532. DOI: 10.3390/rs12213532

Klos, A., Bos, M.S. and Bogusz, J.: 2018, Detecting time-varying seasonal signal in GPS position time series with different noise levels. GPS Solut., 22, 21. DOI: 10.1007/s10291-017-0686-6

Kim, K.Y. and Wu, Q.: 1999, A comparison study of EOF techniques: analysis of non-stationary data with periodic statistics. J. Clim., 12, 1, 185–199. DOI: 10.1175/1520-0442-12.1.185

Li, C., van der Hilst, R.D., Meltzer, A.S., Sun, R. and Engdahl, E.R.: 2008, Subduction of the Indian lithosphere beneath the Tibetan plateau and Burma. Earth Planet. Sci. Lett., 274, 1-2, 157–168. DOI: 10.1016/j.epsl.2008.07.016

Lian, C., Zeng, Z., Yao, W. and Tang, H..: 2012. Displacement prediction model of landslide based on a modified ensemble empirical mode decomposition and extreme learning machine. Nat. Hazards, 66, 2, 759–771. DOI: 10.1007/s11069-012-0517-6

Li, Z., Yue, J.P., Li, W., Lu, D.K. and Li, X.: 2017a, A comparison of hydrological deformation using GPS and global hydrological model for the Eurasian plate. Adv. Space Res., 60, 587–596. DOI: 10.1016/J.ASR.2017.04.023

Li, Z., Yue, J.P., Li, W. and Lu, D.K.: 2017b, Investigating mass loading contributes of annual GPS observations for the Eurasian plate. J. Geodyn., 111, 43–49. DOI: 10.1016/j.jog.2017.07.001

Liu, N., Dai, W., Santerre, R. and Kuang, C.: 2017, A MATLAB-based Kriged Kalman Filter software for interpolating missing data in GNSS coordinate time series. GPS Solut., 22, 1. DOI: 10.1007/s10291-017-0689-3

Montillet, J.-P., Tregoning, P., McClusky, S. and Yu, K.: 2013, Extracting white noise statistics in GPS coordinate time series. IEEE Geosci. Remote Sens. Lett., 10, 10, 563–567. DOI: 10.1109/LGRS.2012.2213576

Ming, F., Yang, Y., Zeng, A. and Jing, Y.: 2016, Analysis of seasonal signals and long-term trends in the height time series of IGS sites in China. Sci. China Earth Sci., 59, 1283–1291. DOI: 10.1007/s11430-016-5285-9

Plaut, G. and Vautard, R.: 1994, Spells of low-frequency oscillations and weather regimes in the northern hemisphere. J. Atmos. Sci., 51, 2, 210–236. DOI: 10.1175/1520-0469(1994)051

Pan, Y. and Shen, W.: 2017, Contemporary crustal movement of southeastern Tibet: constraints from dense GPS measurements. Sci. Rep., 7, 45348. DOI: 10.1038/srep45348

Pan, Y., Shen, W., Shum, C.K. and Chen, R.: 2019, Spatially varying surface seasonal oscillations and 3-D crustal deformation of the Tibetan Plateau derived from GPS and GRACE data. Earth Planet. Sc. Lett., 502, 15, 12–22. DOI: 10.1016/j.epsl.2018.08.037

Raynaud, S., Yiou, P., Kleeman, R. and Speich, S.: 2005, Using MSSA to determine explicitly the oscillatory dynamics of weakly nonlinear climate systems. Nonlin. Process. Geophys., 12, 6, 807–815. DOI: 10.5194/npg-12-807-2005

Ray, J., Altamimi, Z., Collilieux, X. and van Dam, T.: 2008, Anomalous harmonics in the spectra of GPS position estimates. GPS Solut., 12, 1, 55–64. DOI: 10.1007/s10291-007-0067-7

Rangelova, E., Sideris, M. and Kim, J.: 2012, On the capabilities of the multi-channel singular spectrum method for extracting the main periodic and non-periodic variability from weekly GRACE data. J. Geodyn., 54, 64–78. DOI: 10.1016/j.jog.2011.10.006

Styron, R.H., Taylor, M.H. and Sundell, K.E.: 2015, Accelerated extension of Tibet linked to the northward underthrusting of Indian crust. Nature Geosci., 8, 2, 131–134. DOI: 10.1038/ngeo2336

Savage, J.C. and Lisowski, M.: 1993, Inferred depth of creep on the Hayward Fault, Central California. J. Geophys. Res., Atmospheres, 98, 81, 787–793. DOI: 10.1029/92JB01871

Vautard, R., Yiou, P. and Ghil, M.: 1992, Singular spectrum analysis: A toolkit for short, noisy chaotic signals. Phys. D: Nonlinear Phenom., 58, 1, 95–126. DOI: 10.1016/0167-2789(92)90103-T

Walwer, D., Calais, E. and Ghil, M.: 2016, Data-adaptive detection of transient deformation in geodetic networks. J. Geophys. Res., Solid Earth, 121, 3. DOI: 10.1002/ 2015JB012424

Wang, J., He, X. and Ferreira, V.G.: 2015, Ocean wave separation using CEEMD-wavelet in GPS wave measurement. Sensors, 15, 8, 19416–19428. DOI: 10.3390/s150819416

Wang, X., Cheng, Y., Wu, S. and Zhang, K.: 2016, An enhanced singular spectrum analysis method for constructing nonsecular model of GPS site movement. J. Geophys. Res., Solid Earth, 121, 3, 2193–2211. DOI: 10.1002/2015JB012573

Wu, Y., Zhao, Q., Zhang, B. and Wu, W.: 2017, Characterizing the seasonal crustal motion in Tianshan area using GPS, GRACE and surface loading models. Remote Sens., 9, 12, 1303. DOI: 10.3390/rs9121303

Xiang, Y.F., Yue, J.P., Cong, K.L., Xing, Y. and Cai, D.J.: 2019, Characterizing the seasonal hydrological loading over the Asian continent using GPS, GRACE, and hydrological model. Pure Appl. Geophys., 176, 11, 5051–5068. DOI: 10.1007/s00024-019-02251-y

Xu, C. and Yue, D.: 2015, Monte Carlo SSA to detect time-variable seasonal oscillations from GPS-derived site position time series. Tectonophysics, 665, 118–126. DOI: 10.1016/j.tecto.2015.09.029

Xu, C.: 2016. Investigating mass loading contributors of seasonal oscillations in GPS observations using wavelet analysis. Pure Appl. Geophys., 173, 8, 2767–2775. DOI: 10.1007/s00024-016-1301-4

Xu, C.: 2017, Evaluating mass loading products by comparison to GPS array daily solutions. Geophys. J. Int., 208, 1, 24–35. DOI: 10.1093/gji/ggw385

Zhang, B., Liu, L., Khan, S.A., van Dam, T., Zhang, E. and Yao, Y.: 2017, Transient variations in glacial mass near Upernavik Isstrøm (west Greenland) detected by the combined use of GPS and GRACE data. J. Geophys. Res., Solid Earth, 122, 12, 10,626–10,642. DOI: 10.1002/2017JB014529

Zhou, M., Guo, J., Liu, X., Shen, Y. and Zhao, C.: 2020, Crustal movement derived by GNSS technique considering common mode error with MSSA. Adv. Space Res., 66, 8, 1819–1828. DOI: 10.1016/j.asr.2020.06.018